Journal of Physics D: Applied Physics

PAPER

Computational analysis of microstructure-coercivity relation in multi-main-phase Nd–Ce–Fe–B magnets

IOP Publishing

Journal of Physics D: Applied Physics

J. Phys. D: Appl. Phys. **52** (2019) 135002 (8pp)

https://doi.org/10.1088/1361-6463/aaff42

Computational analysis of microstructure-coercivity relation in multi-main-phase Nd–Ce–Fe–B magnets

Dan Liu[1,2], Tianyu Ma[3], Lichen Wang[4], Yanli Liu[1,2], Tongyun Zhao[1,2,5], Fengxia Hu[1,2], Jirong Sun[1,2] and Baogen Shen[1,2,6]

[1] State Key Laboratory of Magnetism, Institute of Physics, Chinese Academy of Sciences, Beijing 100190, People's Republic of China
[2] University of Chinese Academy of Sciences, Beijing 100049, People's Republic of China
[3] Multi-disciplinary Materials Research Center, Frontier Institute of Science and Technology, Xi' an Jiaotong University, Xi' an 710049, People's Republic of China
[4] Department of Physics, Capital Normal University, Beijing 100048, People's Republic of China
[5] Fujian Institute of Innovation, Chinese Academy of Sciences, Fujian 350108, People's Republic of China

E-mail: shenbaogen@yeah.net

Received 7 November 2018, revised 9 January 2019
Accepted for publication 16 January 2019
Published 31 January 2019

Abstract

Multi-main-phase (MMP) (Nd, Ce)$_2$Fe$_{14}$B magnets containing both Nd-rich shell covering Ce-rich core and Ce-rich shell covering Nd-rich core within the 2:14:1 grains have shown much superior coercivity to the single-main-phase ones with homogeneous Nd/Ce distributions. To understand how these core–shell grains and the microstructure of grain boundaries (GBs) influence the coercivity of MMP Nd–Ce–Fe–B magnets, micromagnetic simulation was carried out through constructing a 3D finite element model. The influences of physical dimension and magnetism of the GBs, Nd or Ce-rich shell thickness, and Ce substitution level on coercivity were all analyzed. It was found that thick and nonmagnetic GB layers play an essential role in enhancing the coercivity as the intergrain exchange coupling can be weakened. Thicker Nd-rich or Ce-rich 2:14:1 grain shells are not necessary for enhancing the coercivity. In addition, with the increase of Ce content, the coercivity does not deteriorate linearly but exhibits an abnormal enhancement around 20 vol.% substitution. The good agreement with the experiments makes these findings as important insights of understanding the coercivity mechanism of MMP RE–Fe–B magnets.

Keywords: abundant rare earth, permanent magnets, multi-main-phase magnets, micromagnetic simulation

(Some figures may appear in colour only in the online journal)

1. Introduction

The high energy product of Nd$_2$Fe$_{14}$B-based sintered magnet has made it an attractive material for applications in various motors, generators and acoustics devices [1–4]. However, the rapidly increasing consumption of Nd–Fe–B magnets results in skyrocketing prices and overusing of Nd, Pr, Dy and Tb rare earths (RE). In order to balance the utilization of the RE resources reasonably and to raise economic efficiency, great efforts have been made to substitute cheap and abundant RE elements such as Ce, La, and Y for Nd in the Nd–Fe–B magnets [5, 6]. Among them, the most abundant and the cheapest RE element Ce has gained considerable interest. However, Ce substitution for Nd in the 2:14:1 phase lattice inevitably

[6] Author to whom any correspondence should be addressed.

deteriorates the magnetic properties since the intrinsic magnetic properties of $Ce_2Fe_{14}B$ are far inferior to those of $Nd_2Fe_{14}B$ [3].

There has been an intense worldwide research aim to solve the big challenge to fabricate high magnetic performance Nd–Ce–Fe–B magnets with high Ce substitution level. Among them, recent work suggested that co-sintering Nd–Fe–B and Nd–Ce–Fe–B powders is a feasible approach to fabricate high cost-performance permanent magnets [7–11]. In comparison with the SMP magnets prepared by sintering the single type Nd–Ce–Fe–B powders, the co-sintered magnets with multi-main-phase (MMP) grains possess much superior magnetic performance, especially significantly enhanced coercivity, at the same average composition. For example, the maximum energy product $(BH)_{max}$ can be maintained to 202.1 kJ m^{-3}even when 45 wt.% Nd is substituted by Ce in the MMP Nd–Ce–Fe–B magnets [10]. In addition, with the same Ce substitution content of 20 wt.%, the coercivity is dramatically enhanced from 612.7 kA m^{-1} for the SMP Nd–Ce–Fe–B magnet to 962.9 kA m^{-1} for the MMP one [12].

In order to further enhance the coercivity of high Ce-containing MMP Nd–Ce–Fe–B magnets to be comparable of that for commercial Nd–Fe–B magnets, the latest studies focused on the coercivity mechanism of such magnets with complex microstructure features [13–15]. Both SMP and MMP magnets have similar morphologies, the magnetically hard 2:14:1 main phase grains are separated by RE-rich intergranular phase. Unlike the SMP magnets where RE element distributes homogeneously inside the 2:14:1 grains, the MMP magnets contain grains with locally different RE element distributions, namely the Ce-rich core covered by Nd-rich shell and the Nd-rich core covered by Ce-rich shell. A recent investigation through annealing the MMP Nd–Ce–Fe–B magnets at different temperatures, Zhang and Ma *et al* [13, 15] have suggested that the inhomogeneous Nd/Ce distributions within the main phase grains and the formation of continuous grain boundary (GB) layers should be balanced to optimize the coercivity. Following this scenario, they further introduced (Nd, Pr)-H powders to restructure the grain boundaries (GBs) of the MMP Nd–Ce–Fe–B magnets and have successfully raised the coercivity above 954.9 kA m^{-1} with 40 wt.% Ce substitution [14]. Despite that these investigations have suggested an ideal microstructure for achieving high coercivity in the MMP magnets, the underlying mechanism of how such complex microstructure and the resultant complex magnetic interactions among the 2:14:1 phases influence the nucleation and propagation of reverse magnetic domains is not fully understood. The main difficulty arises from the direct observation of magnetization reversal under external field in real-time, especially the confirmation of primary position of reverse domain nucleation during the demagnetization process. Besides, it is difficult to exactly measure the thickness of Nd- and/or Ce-rich 2:14:1 phase shells experimentally. Consequently, computational simulation may provide an alternative approach to produce a more reasonable understanding of the coercivity mechanism.

Micromagnetic simulation has been concerned as an effective way to investigate the relationship between the macroscopic properties and the microstructures of Nd–Fe–B magnets at mesoscopic scale [16]. In this work, the influences of varying microstructure of GBs and local compositions of the main phase on the magnetic properties were then investigated by micromagnetism finite element method. A well-defined 3D model with core–shell microstructures is created by the Voronoi tessellation. According to the micromagnetic simulations, the magnetic properties of MMP Nd–Ce–Fe–B magnets with two kinds of core–shell structures are investigated in detail. Our simulation results agree well with the experiment results [14, 17], which might provide a clear guidance for developing alternative and economically attractive permanent magnets.

2. Method

Micromagneticsm finite element method has made great achievements on the researches of magnetic behavior of Nd–Fe–B magnets [18, 19]. The micromagnetic simulation is based on the principle of static micromagnetic theory and a more detailed description of the method used has been given in [20]. By means of finite element method, the total magnetic Gibbs free energy (E_{tot}) can be expressed by formula (1), in which E_{exc}, E_{ani}, E_d, and E_{ext} are exchange energy, magnetocrystalline anisotropy energy, demagnetization energy, and Zeeman energy, respectively.

$$E_{tot} = E_{exc} + E_{ani} + E_d + E_{ext}, \tag{1}$$

$$E_{tot} = \int \left\{ A\left[(\nabla \boldsymbol{m_x})^2 + (\nabla \boldsymbol{m_y})^2 + (\nabla \boldsymbol{m_z})^2 \right] - K_1 \boldsymbol{m_z}^2 - \frac{1}{2}\mu_0 \boldsymbol{M}\cdot\boldsymbol{H_d} - \mu_0 \boldsymbol{M}\cdot\boldsymbol{H_{ext}} \right\} \mathrm{d}V. \tag{2}$$

The magnetization $\boldsymbol{M}$ describes the state of magnet which is a continuous function of position. And $\boldsymbol{m} = \boldsymbol{M}/M_s$ is the component of magnetization relative to the field direction. Here A is the exchange constant, K_1 is the anisotropy constant and V is the total volume of magnetic material. In order to find the equilibrium magnetization configuration of the magnet, E_{tot} is minimized with respect to the direction of the spontaneous magnetization. The Brown equation describes the mathematical relationships between the magnetization and effective field in equilibrium magnetization state:

$$\boldsymbol{m} \times \boldsymbol{H_{eff}} = 0. \tag{3}$$

The effective field $\boldsymbol{H}_{eff} = -\partial E_{tot}/\partial \boldsymbol{M}$ is an equivalent field of the total Gibbs free energy that influences on the magnetization vector:

$$\boldsymbol{H_{eff}} = \frac{2A}{M_S}\nabla^2 \boldsymbol{m} + \mu_0 \boldsymbol{H_d} + \mu_0 \boldsymbol{H_{ext}} - \frac{1}{M_S}\frac{\partial w_{ani}}{\partial \boldsymbol{m}}. \tag{4}$$

Where μ_0 is the permeability of free space and w_{ani} is the energy associated with magnetocrystalline anisotropy. The coefficients A and K_1 in the equation vary with position and thus represent the chemical inhomogeneity of the real magnet.

In this work, modeling of multi-grain microstructure is based on Voronoi tessellation method [21]. In general, the locations of the generators of the Voronoi tessellation do not

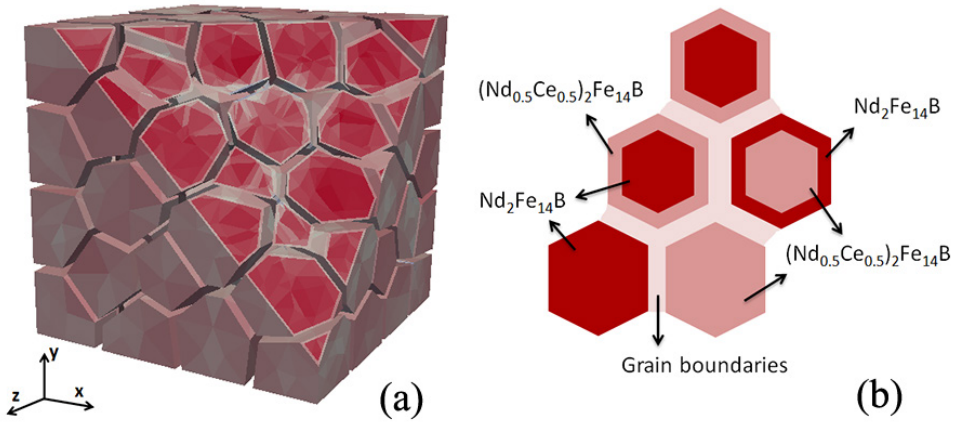

Figure 1. (a) A polycrystalline model of MMP Nd–Ce–Fe–B magnets created by the Voronoi tessellation method. (b) Schematic diagram of the two kinds of grains with core–shell Nd/Ce distributions. The model size is $3000 \times 3000 \times 3000\,nm^3$, containing 100 irregularly shaped grains.

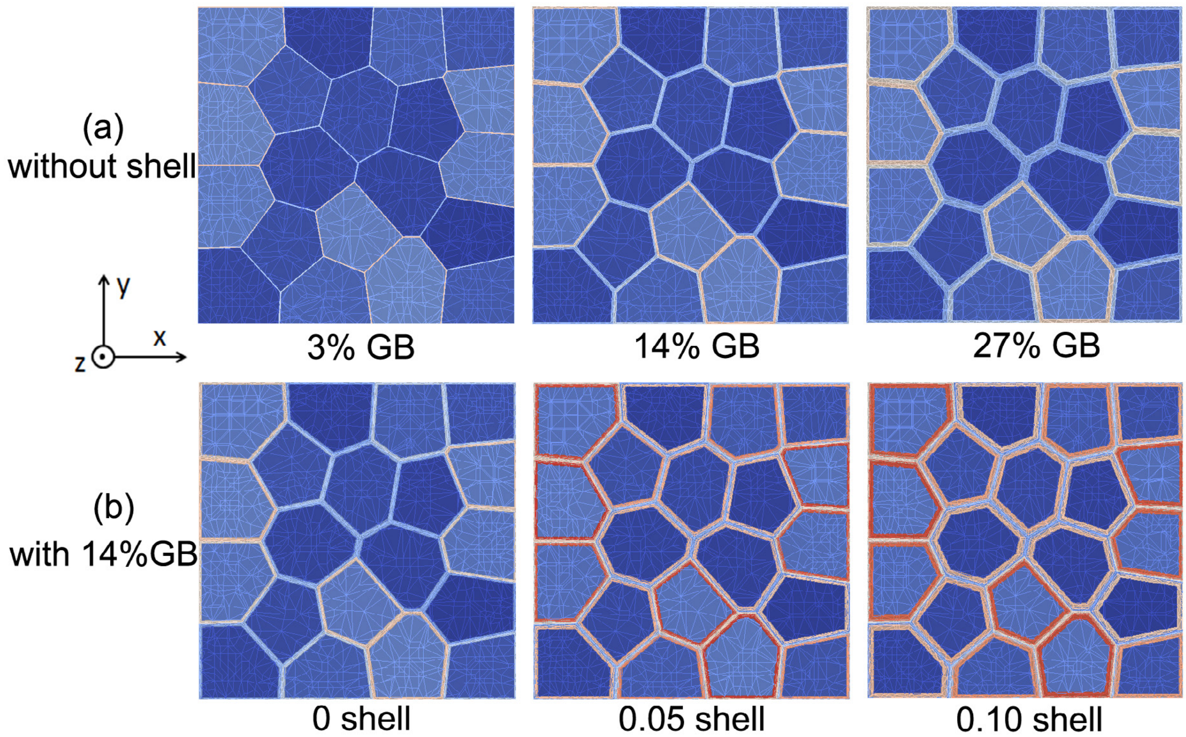

Figure 2. The microstructures and wireframes of the simulation models. (a) Different GB volume fractions without core–shell Nd/Ce distributions. (b) Different shell thicknesses of the 2:14:1 phase grains for the magnets with 14 vol.% GB phase. The shell thickness is represented by its ratio with respect to the grain size.

coincide with the centers of mass of the corresponding Voronoi regions. It not only leads to abnormal formation of regions but also brings inconvenience to the calculation. Therefore, a centroidal Voronoi tessellation whose generating points are also the mass centers is constructed by Neper [22]. 3D finite element micromagnetic simulation software Magpar [23] is performed to investigate the magnetization reversal mechanism in the MMP Nd–Ce–Fe–B magnets. The macroscopic shape of the model is a cube with the edge length of 3000 nm. It contains 100 irregular grains. The grain size is smaller than those of the real sinter magnets due to the limit of computing capability, but the cuboidal model well representative to the actual particle shape. To better imitate the actual grains observed in the real magnets, grain models are constructed in two varieties: a softer $(Nd_{0.5}Ce_{0.5})_2Fe_{14}B$ grain core covered with a harder $Nd_2Fe_{14}B$ shell and a $Nd_2Fe_{14}B$ grain core covered with a $(Nd_{0.5}Ce_{0.5})_2Fe_{14}B$ shell. The model in figure 1(a) is assumed for the simulation and the external field is along *z*-axis. Figure 1(b) is the heterogeneous microstructure composed of grains with distinctly different mean composition. Each grain is surrounded by GBs with equivalent thickness.

The GB phase and the shells in the 2:14:1 main phase grains are created by shrinking each grain with respect to its Voronoi generating point. The finite element mesh generation is achieved by the grid generator Gmsh [24]. For a series of cases with the volume fraction of GB phase of 3%, 9%, 14%,

Table 1. The magnetic properties of RE–Fe–B magnets used in simulations.

	Anisotropy constant K_1 (MJ m^{-3})	Saturation magnetization J_s (T)	Exchange stiffness A (pJ m^{-1})
$Nd_2Fe_{14}B$	4.3	1.61	7.7
$Ce_2Fe_{14}B$	1.5	1.17	5

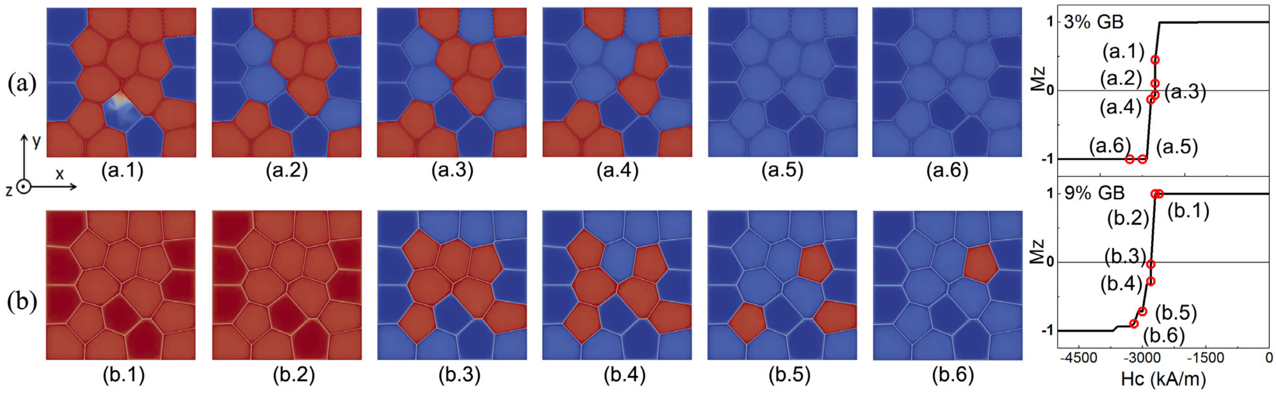

Figure 3. Magnetization reversal patterns of MMP Nd–Ce–Fe–B magnets for the cases with different volume fractions of GB phase. (a) 3% and (b) 9%. The magnetization in z-direction is represented by regions in red ($+z$) and blue ($-z$). (c) The corresponding demagnetization curves.

22%, and 27%, the corresponding thickness of the GB layer is about 4 nm, 12 nm, 20nm, 32 nm, and 40 nm, respectively. The thickness of Nd- or Ce-rich 2:14:1 shell is represented by the ratio of shell width to the mean grain size. For instance, 0.05 shell means that the shell thickness is 5% of the grain radius. Here we suppose that thickness of the $Nd_2Fe_{14}B$ shell and the $(Nd_{0.5}Ce_{0.5})_2Fe_{14}B$ shell is equivalent to each other in all grains. For investigating the Ce substitution content influence, we changed the ratio between the $Nd_2Fe_{14}B$ and the $(Nd_{0.5}Ce_{0.5})_2Fe_{14}B$ grains. As shown in figure 2, the GB thickness and the shell thickness are changed separately to investigate the microstructure-coercivity relation. The material parameters of $Nd_2Fe_{14}B$ and $Ce_2Fe_{14}B$ are tabulated in table 1 [25, 26]. The parameters for $(Nd_{0.5}Ce_{0.5})_2Fe_{14}B$ are obtained by using a linear interpolation between the values of these two extreme compositions. Both nonmagnetic and ferromagnetic GB layers are considered for comparison. With the optimization of computer hardware and numerical methods, the magnetization reversal behavior of magnets can be computed clearly.

3. Results and discussion

Shown in figure 3 are representative simulation results for two MMP Nd–Ce–Fe–B magnets with different volume fractions of GB phase. The volume ratio of the $Nd_2Fe_{14}B$ and the $(Nd_{0.5}Ce_{0.5})_2Fe_{14}B$ grains is 1:4, the thickness of both Ce-rich and Nd-rich 2:14:1 shells inside each grain is 0.1. The GB is thought of nonmagnetic. Our simulated results show that the MMP Nd–Ce–Fe–B magnets exhibit a gradual magnetization reversal process during demagnetization. The reversed domains (blue contrast) propagate from one grain to another, but the magnetization reversal occurs preferably inside the $(Nd_{0.5}Ce_{0.5})_2Fe_{14}B$ grains (for which the reversed domains are in dark blue), which is prior to that inside the $Nd_2Fe_{14}B$ grains

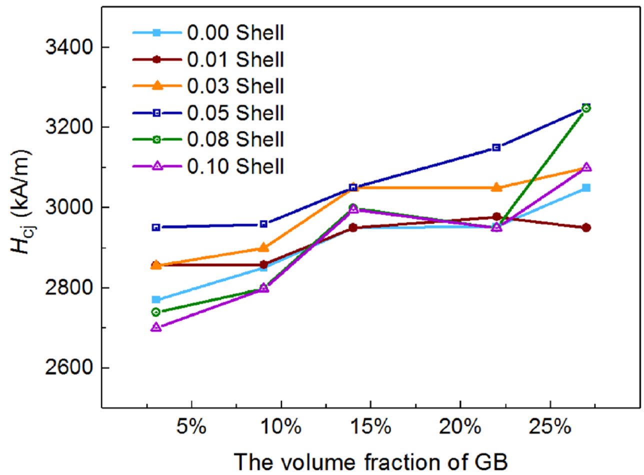

Figure 4. Dependence of coercivity on the GB thickness for MMP Nd–Ce–Fe–B magnets with different three different shell-structures.

(for which the reversed domain are in light blue). Especially, in figure 3(a.1), a grain in the center region contains partially reversed domains, indicating that the magnetization reversal inside one individual 2:14:1 grain is also a gradual propagation process due to the difference of chemical composition between the core and the shell regions. Since it is hard to reveal the nucleation site experimentally, here time-resolved simulations are carried out to unveil this issue. With prolonging the time, the magnetization reversal propagate across grains (from the $(Nd_{0.5}Ce_{0.5})_2Fe_{14}B$ grains to the $Nd_2Fe_{14}B$ ones), which can be seen from a series of simulated patterns in figures 3(a.1)–(a.5). The magnetization reversal finishes (figure 3(a.5)) at the coercive field where the magnetization reaches zero in the simulated demagnetization curve.

Furthermore, the magnetization reversal process is very sensitive to the thickness of GBs. When the boundary phase layer is extremely thin (figure 3(a)), the nucleation occurs at

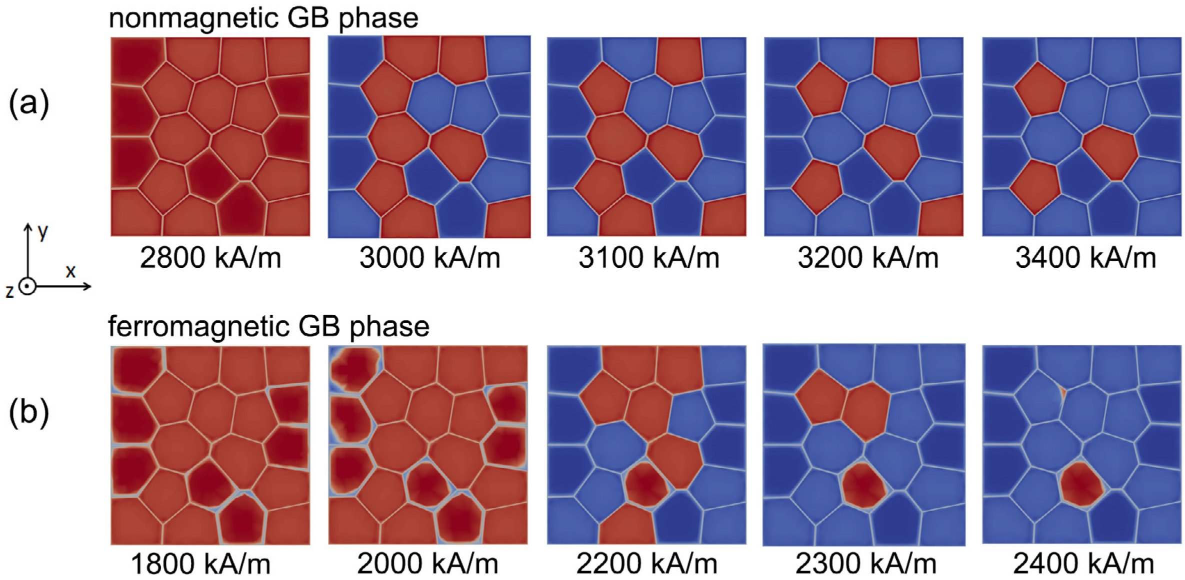

Figure 5. The magnetization reversal diagrams of magnets with (a) nonmagnetic ($J_s = 0$ T) and (b) weakly ferromagnetic ($J_s = 0.8$ T) GB layers at different shell thickness. The volume fraction of GB phase used here is 14%.

the soft phase at the beginning of the reversal processes. And then the reversed magnetic domains spread rapidly, which lead to a reduction of the coercive field. In figure 3(b), the reverse domains start to nucleate at the grains on the surface of the magnets. When the reverse domains expand to the interface, the pinning of thick GB significantly hinders their movements. As the figure shows the grains are switched individually. In comparison with the case with a thinner GB (figure 3(a)), the MMP magnet with thicker nonmagnetic GBs has a higher coercivity. As shown in figure 3(b), a series of magnetic configurations directly reveal that the magnetization reversal at the same time is much slower for the latter than that for the former. For example, in figures 3(b.1) and 3(b.2), the nucleation of reverse domains even does not happen, unlike the case with a thinner GB. In addition, the magnetization reversal is still not complete as shown in figure 3(b.5), which is obtained at the same time with that in figure 3(a.5), for which the magnetization reversal process has been finished. Such difference indicates that (i) the nucleation of reverse domain starts at a higher opposite external field and (ii) the magnetization reversal across grains is slower if the GBs are thicker. It is due to the fact that thick nonmagnetic GBs may weaken the short-range exchange coupling between adjacent 2:14:1 grains [27], which helps to prevent the rapid propagation of reverse domains across them. The comparison highlights the importance of forming a thicker nonmagnetic GB for achieving higher coercivity in MMP Nd–Ce–Fe–B magnets.

The GB phase layer is of crucial importance in double main phase system. Therefore, the volume fraction of GB phase was further changed from 3% to 27% for a more systematic study. Higher volume fraction of GB phase is not consistent with the actual situation and will not be considered here. Figure 4 illustrates the effect of GB on coercivity under different core–shell structures. The ratio of the Nd-rich grains and the Ce-rich grains in all magnets is set to be 1:4. The coercivity overall shows an upward trend with the increase of GB phase in a certain range. It proves that the coercivity field has been enhanced by the existence of GB phase. Indicated by simulation results in figure 3(b), the distribution of the GB phase between the grains led to the phase separation, which influences the nucleation of reversed domain. When the phases are contacted with no or thin GB phases, the exchange coupling is enhanced, leading to losing coercivity eventually. However, the coercivity will increase when the grains of the granular system are separated by clear GB phases. The phase segregation phenomenon in MMP magnet is related to magnetic performance which was also to be found by Pathak *et al* [10]. The exchange coupling between grains is weakened after GB restructuring, giving rise to significantly enhanced coercivity.

The coercivity is not only dependent on the microstructure, but also the intrinsic magnetic properties of GB phase. Figure 5 is the magnetization reversal process of magnets with (a) nonmagnetic and (b) weakly ferromagnetic GB layers under different external magnetic fields. The volume fraction of GB phase used here is 14% and the thickness of shell is 0.1. With the fixed structure of model, the saturation magnetic polarization of GB phase is changed from 0 T to 0.8 T. The simulation result shows the coercivity is much higher for the MMP Nd–Ce–Fe–B magnet if the grains are separated by nonmagnetic GB layers ($H_{cj} = 3.0 \times 10^3$ kOe) than that with soft magnetic GBs ($H_{cj} = 2.2 \times 10^3$ kOe). Such enhancement is due to the weakened exchange coupling effect between the adjacent grains. By comparing the patterns of the magnetization reversal of two kinds of magnets, the influence of material parameters of GB phase on demagnetization processes is investigated. In both models, the magnetization switch begins at the position with lower anisotropic around the edge. When the GBs are nonmagnetic phases (figure 5(a)), the magnetic domains in different grains turn over independently. The GB phase acts as an isolation which is similar to the previous simulation result (figure 3(b)). However, when the GBs are

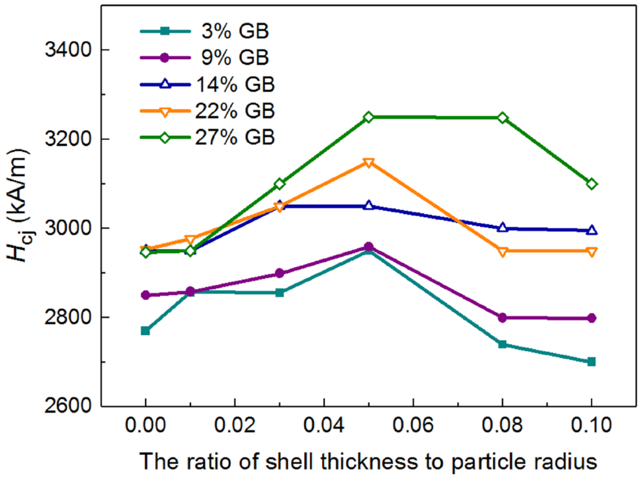

Figure 6. The dependence of coercivity on the shell thickness with the various volume fraction of GB phase. The GB phase is set to be an amorphous non-ferromagnetic layer.

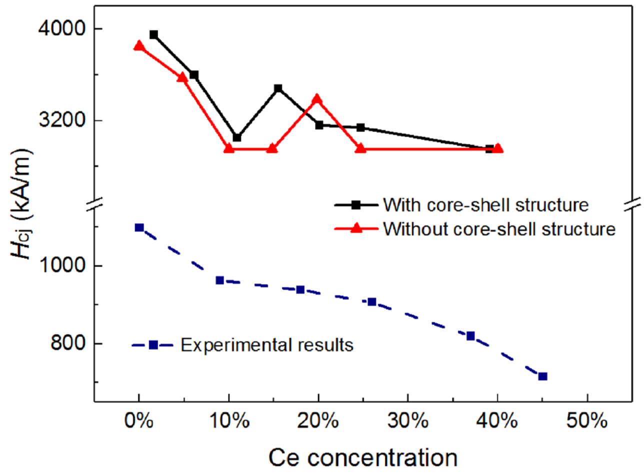

Figure 7. Coercivity field as a function of Ce Concentration for the model with a thin shell structure and without shell structure. The volume fraction of GB phase used here is 14%. The blue dotted line is the coercivity curve of real magnets with different Ce substituted.

magnetic phases (figure 5(b)), the magnetic domains of grains prefer to be reversed as a whole under the external magnetic field once the reverse magnetization nucleus is formed. Even though the GB is pretty thick, the magnetization reversal mechanism of the model with ferromagnetic GB phase is similar to figure 3(a). The simulation results illustrate the importance of a continuous and nonferromagnetic GB phase. According to the researches [28–30], the presence of ferromagnetic GB phase will induce the rapid and extensive spread of the magnetic moments in sintered magnets. While the concentration of RE and Fe affects the ferromagnetism of the GB phase. It implies that enriching RE elements or reducing Fe content can increase the coercivity by weakening exchange coupling between grains.

High performance Nd–Fe–B magnets without any heavy rare earth can be achieved by GB diffusion [15]. When the boundaries between two main phases infiltrate each other, the structures of grains change to the core–shell structures. The influence of diffusion degree on the coercivity performance of core–shell structure is studied by changing the thickness of shell. The ratio of two phases remains constant 1:4 as before and the GB is assumed to be nonmagnetic. The dependence of coercivity on the shell thickness with different GB thickness can be seen in figure 6. The coercivity of the magnets increases with the increasing diffusion depth from about 0 to 0.05, and after that it shows a minor decrease from 0.05 to 0.1. When the grains turn into core–shell structure after diffusion, the coercivity of the magnet significantly changed, indicating that the $(Nd,Ce)_2Fe_{14}B$ shells are critical to coercivity. It is expected that the formation of a high anisotropy shell surrounding the Ce-rich 2:14:1 core can enhance the coercivity. Moreover, the core–shell structure separates the grains from each other, which could increase the coercivity through weakening the interaction between the grains. However, figure 6 also shows that the deep diffusion may be not necessary for the core–shell structure. This could be due to the gradual homogenization which caused by the over-thick shell [14].

The above results highlight the importance of constructing core–shell Nd/Ce distribution for enhancing the coercivity of Nd–Ce–Fe–B magnets. The suitable thickness of shell is helpful in improving the magnetic performance and that may be one reason for two main phase magnets performs much better than SMP ones. Experimentally, Nd–Ce–Fe–B magnets consisting of core–shell grains separated by a non-magnetic GB phase can be fabricated by GB diffusion process. For real magnets, the diffusion processes seem to be very much dependent on surface quality and the nature of the contact between diffusion source and magnet [15]. And the competition contributions between the formation of shell-structure and the chemical heterogeneity should be balanced. Therefore, the shell thickness should be well controlled to maintain good magnetic properties.

The influences of Ce content on the coercivity of Nd–Ce–Fe–B magnets are shown in figure 7. The volume fraction of the nonmagnetic GB phase is 14% for all the modles. The only difference between these two computing model is the grain structure used for the simulation. One is a model without shell, and the other is a model with a shell thickness of 0.01. The coercivity of the magnet with core–shell structure is higher than that without core–shell structure. It shows that the formation of a thin shell is beneficial to maintain the high performance during doping process, which coincides with the former simulation results. As we can see in figure 7, the coercivity decreases with the increase of Ce content firstly, followed by a slight recovery and then continues to decline. The simulation results suggest that the coercivity is effectively changed by the ratio of two kinds of main phase. A little additive amount of $Ce_2Fe_{14}B$ results in a dramatic drop of coercivity, which indicates that coercivity is sensitive to replacement. Similar to previous simulation results [31], the magnetic properties do not decrease monotonously with the increase of Ce proportion. The abnormality of coercivity with an appropriate Ce concentration is also to be found in this

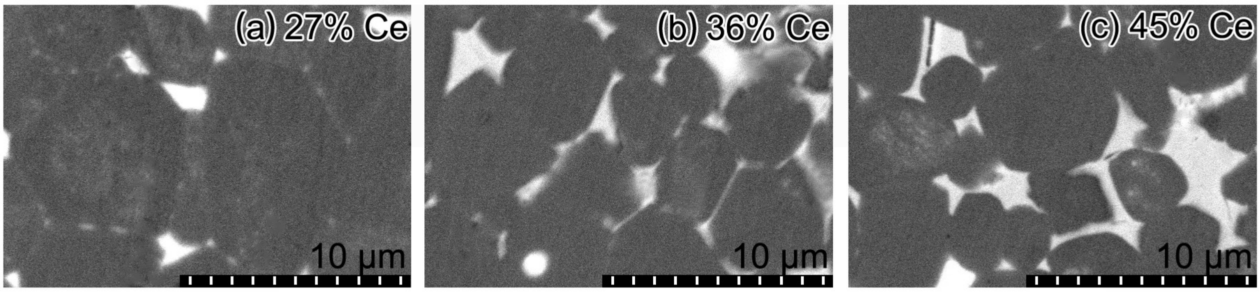

Figure 8. Back-scattered SEM images of the magnets with different Ce substitution amounts: (a) 27%, (b) 36%, and (c) 45%. The dark part corresponds to the main phase, while the bright contrast corresponds to the GB phase.

case, approximately when the percentage of doped cerium is 20%. Although the locations of the abnormal peak are slightly different, the simulation curves of both models all display the value anomalies. The comparative study demonstrates that the abnormal increase in the value of coercivity is mainly related to GB phase, not the core–shell structure of grains.

The influence of Ce content on magnets is further studied experimentally. By adjusting the mixing ratio of raw materials, the composition of Ce could be controlled. The MMP Nd–Ce–Fe–B magnets with the nominal composition of $(Pr,Nd)_{31.3}(Fe,M)_{bal}B_{0.98}$, $[(Pr,Nd)_{0.91}Ce_{0.09}]_{31.3}(Fe,M)_{bal}B_{0.98}$, $[(Pr,Nd)_{0.82}Ce_{0.18}]_{31.3}(Fe,M)_{bal}B_{0.98}$ $[(Pr,Nd)_{0.73}Ce_{0.27}]_{30.5}Fe_{bal}M_{1.0}B_{1.0}$, $[(Pr,Nd)_{0.64}Ce_{0.36}]_{30.5}Fe_{bal}M_{1.0}B_{1.0}$, and $[(Pr,Nd)_{0.55}Ce_{0.45}]_{30.5}Fe_{bal}M_{1.0}B_{1.0}$ (M = Al, Cu, Ga, Zr, wt.%) were obtained by dual alloy method. The Ce accounts for 0%, 9%, 18%, 27%, 36%, and 45% of the total rare earth content respectively. The main technological processes are standard strip-casting, hydrogen decrepitating, jet milling, compaction of powder under magnetic field, and sintering. The samples used here are the same as those used in the microstructure analysis by Ma *et al* [14], and the detail experimental procedure is specified in the literature. Figure 7 is the variation trend of coercivity with Ce content. As we all know, the coercivity of typical Nd–Fe–B sintered magnets is only about 20% of the anisotropy field of the $Nd_2Fe_{14}B$ phase [32]. The coercivity obtained from simulation is larger than that of the actual magnet which demonstrates the coercivity of Nd–Ce–Fe–B MMP magnet can be further enhanced by forming a better microstructure. In general, Ce substitution leads to seriously destroy the spontaneous magnetization and magnetocrystalline anisotropy of magnets because of the saturation magnetization of $Ce_2Fe_{14}B$ is 26% lower than of $Nd_2Fe_{14}B$, and the anisotropy field is 3 times lower [3]. Although there is no obvious abnormal increase of H_{cj} observed in figure 7 (the dotted line), the decline rate is remarkably slow down around 20% Ce-doping. The coercivity of Ce18% magnet is almost identical to the Ce9% magnet. Furthermore, the magnetic square degree of Ce-18 is even better than Ce-9 at all sintering temperatures [17]. It indicated that the proper amount of Ce has a positive effect on the magnetic properties of two-phase magnets.

A scanning electron microscope equipped with an Auger electron spectrometer is used to observe the microstructure of the magnets. Figure 8 is the back-scattered SEM images of the magnets with different Ce substitution amounts. There is a significant increase in the volume fraction of GB phase and a slight reduction in grain size with the increase of Ce content. In contrast to the main phase, the low-melting GB phase may be more conducive to optimizing microstructure and maintaining magnetic energies in the Nd–Ce–Fe–B MMP magnets. Combined with the results of the elemental concentration distribution [14], the RE-rich phase will be more evenly distributed along GB during sintering. The interfacial exchange coupling between adjacent grains can be reduced by the formation of continuous GBs so that the magnetic dilution effect caused by the soft phase can be suppressed. Therefore, the elevated coercivity provides a partial compensation for the coercivity loss caused by soft phase. The experiment results are well accord with the ones obtained in simulation, which indicate that the theoretical models describe the MMP magnets system correctly and offer guidance to the GB design.

4. Conclusions

The magnetic properties of MMP Nd–Ce–Fe–B magnets with the core–shell structure are analyzed by Computer simulations based on micromagnetic method. A finite element program has been developed to calculate the magnetic behavior in a given microstructure. Micromagnetic simulations revealed a strong dependency of magnetic properties on the microstructure and content of magnets. In the process of magnetization reversal induced by magnetic field, the existence of GB phase will change the coupling between grains and have a significant influence on the coercive force of magnets. Excellent hard magnetic properties can be achieved in GB engineered magnets. The analysis also suggests that the coercivity can be further enhanced if the GB is nonmagnetic. The effect of dimensional change of shell on the magnetization reversal is investigated. It is found that only a limited diffusion depth is needed to enhance the coercivity for a magnet. Besides, there is an abnormally increase of coercivity around 20% Ce doped MMP Nd–Ce–Fe–B magnets and it might be related to the GBs. The theoretical and experimental results have revealed the possibility to gain high performance permanent magnets with low-cost rare earth elements, and provide a promising approach to design and optimize of the experimental setup and manufacturing process.

Acknowledgments

This work was supported by the National Natural Science Foundation of China (Grant Nos. 51590880 and 51622104); the National Key Research and Development Program of China (Grant Nos. 2014CB643702 and 2016YFB0700903); the Inner Mongolia Science and Technology Major Project of China 2016; and the Key Research Program of the Chinese Academy of Sciences of China (Grant No. KJZD-EW-M05). We thank Prof Mi Yan and Dr Yujing Zhang of Zhejiang University for kind help.

ORCID iDs

Dan Liu https://orcid.org/0000-0003-4002-0690
Tianyu Ma https://orcid.org/0000-0003-4637-0667
Baogen Shen https://orcid.org/0000-0002-8369-1526

References

[1] Croat J J, Herbst J F, Lee R E and Pinkerton F E 1984 Pr–Fe and Nd–Fe-based materials: a new class of high-performance permanent magnets *J. Appl. Phys.* **55** 2078–82
[2] Gutfleisch O, Willard M A, Brück E, Chen C H, Sankar S G and Liu J P 2011 Magnetic materials and devices for the 21st century: stronger, lighter, and more energy efficient *Adv. Mater.* **23** 821–42
[3] Sugimoto S 2011 Current status and recent topics of rare-earth permanent magnets *J. Phys. D. Appl. Phys.* **44** 110–18
[4] McCallum R W, Lewis L H, Skomski R, Kramer M J and Anderson I E 2014 Practical aspects of modern and future permanent magnets *Annu. Rev. Mater. Res.* **44** 451–77
[5] Li Z B, Shen B G, Zhang M, Hu F X and Sun J R 2015 Substitution of Ce for Nd in preparing $R_2Fe_{14}B$ nanocrystalline magnets *J. Alloys Compd.* **628** 325–8
[6] Li Z, Liu W Q, Zhang S S, Li Y Q, Wang Y Q, Zhang D T, Yue M, Zhang J X and Huang X L 2015 Effects of CE substitution on the microstructures and intrinsic magnetic properties of Nd–Fe–B alloy *J. Magn. Magn. Mater.* **393** 551–4
[7] Herbst J F, Meyer M S and Pinkerton F E 2012 Magnetic hardening of $Ce_2Fe_{14}B$ *J. Appl. Phys.* **111** 07A718
[8] Pathak A K, Khan M, Gschneidner K A Jr, McCallum R W, Zhou L, Sun K, Kramer M J and Pecharsky V K 2016 Magnetic properties of bulk, and rapidly solidified nanostructured $(Nd_{1-x}Ce_x)_2Fe_{14-y}Co_yB$ ribbons *Acta. Mater.* **103** 211–6
[9] Betancourt R J I and Davies H A 2002 Effect of the grain size on the magnetic properties of nanophase REFeB alloys *J. Magn. Magn. Mater.* **246** 6–9
[10] Zhang Y J, Ma T Y, Jin J Y, Li J T, Wu C, Shen B G and Yan M 2017 Effects of $REFe_2$ on microstructure and magnetic properties of Nd–Ce–Fe–B sintered magnets *Acta Mater.* **128** 22–30
[11] Pathak A K *et al* 2015 Cerium: an unlikely replacement of dysprosium in high performance Nd–Fe–B permanent magnets *Adv. Mater.* **27** 2663–7
[12] Zhu M G, Han R, Li W, Huang S L, Zheng D W, Song L W and Shi X N 2015 An enhanced coercivity for (CeNdPr)–Fe–B sintered magnet prepared by structure design *IEEE Trans. Mag.* **51** 1–4
[13] Zhang Y J, Ma T Y, Yan M, Jin J Y, Wu B, Peng B X, Liu Y S, Yue M and Liu C Y 2018 Post-sinter annealing influences on coercivity of multi-main-phase Nd–Ce–Fe–B magnets *Acta Mater.* **146** 97–105
[14] Ma T Y, Yan M, Wu K Y, Wu B, Liu X L, Wang X J, Qian Z Y, Wu C and Xia W X 2018 Grain boundary restructuring of multi-main-phase Nd–Ce–Fe–B sintered magnets with Nd hydrides *Acta Mater.* **142** 18–28
[15] Ma T Y, Zhang W Y, Peng B X, Liu Y S, Chen Y J, Wang X H and Yan M 2018 Magnetic performance change of multi-main-phase Nd–Ce–Fe–B magnets by diffusing (Nd, Pr)H_x *J. Phys. D: Appl. Phys.* **51** 055003
[16] Helbig T, Loewe K, Sawatzki S, Yi M, Xua B X and Gutfleisch O 2017 Experimental and computational analysis of magnetization reversal in (Nd,Dy)–Fe–B core shell sintered magnets *Acta Mater.* **127** 498–504
[17] Zhang Y J 2017 *High Performance Permanent Magnets Based on Cheap and Abundant Rare Earths* (Hangzhou: Zhejiang University)
[18] Fischer R, Leineweber T and Kronmüller H 1998 Fundamental magnetization processes in nanoscaled composite permanent magnets *Phys. Rev.* B **57** 10723–32
[19] Zhang H W, Rong C B, Du X B, Zhang S Y and Shen B G 2004 Investigation on the coercivity and remanence of single-phase nanocrystalline permanent magnets by micromagnetic finite-element method *J. Magn. Magn. Mater.* **278** 127–37
[20] Hertel R 2001 Micromagnetic simulations of magnetostatically coupled Nickel nanowires *J. Appl. Phys.* **90** 5752–8
[21] Du Q, Faber V and Gunzburger M 1999 Centroidal voronoi tessellations: applications and algorithms *SIAM Rev.* **41** 637–76
[22] Quey R, Dawson P R and Barbe F 2011 Large-scale 3D random polycrystals for the finite element method: generation, meshing and remeshing *Comput. Methods Appl. Mech. Eng.* **200** 1729–45
[23] Scholz W, Fidler J, Schrefl T, Suess D, Dittrich R, Forster H and Tsiantos V 2003 Scalable parallel micromagnetic solvers for magnetic nanostructures *Comput. Mater. Sci.* **13** 366–83
[24] Geuzaine C and Remacle J F 1997 Gmsh: a three-dimensional finite element mesh generator with built-in pre-and post-processing facilitiesInt *Int. J. Numer. Methods Eng.* **79** 1309–31
[25] Schrefl T, Fischer R, Fidler J and Kronmüller H 1994 Two- and three-dimensional calculation of remanence enhancement of rare-earth based composite magnets *J. Appl. Phys.* **76** 7053–8
[26] Herbst J F 1991 $R_2Fe_{14}B$ materials: intrinsic properties and technological aspects *Rev. Mod. Phys.* **63** 819–98
[27] Jin J Y, Wang Z, Bai G H, Peng B X, Liu Y S and Yan M 2018 Microstructure and magnetic properties of core–shell Nd–La–Fe–B sintered magnets *J. Alloys Compd.* **749** 580–5
[28] Murakami Y, Tanigaki T, Sasaki T T, Takeno Y, Park H S, Matsuda T, Ohkubo T, Hono K and Shindo D 2014 Magnetism of ultrathin intergranular boundary regions in Nd–Fe–B permanent magnets *Acta Mater.* **71** 370–9
[29] Kohashi T, Motai K, Nishiuchi T and Hirosawa S 2014 Magnetism in grain-boundary phase of a NdFeB sintered magnet studied by spin-polarized scanning electron microscopy *Appl. Phys. Lett.* **104** 232408
[30] Nakamura T *et al* 2014 Direct observation of ferromagnetism in grain boundary phase of Nd–Fe–B sintered magnet using soft x-ray magnetic circular dichroism *Appl. Phys. Lett.* **105** 202404
[31] Liu D, Zhao T Y, Li R, Zhang M, Shang R X, Xiong J F, Zhang J, Sun J R and Shen B G 2017 Micromagnetic simulation of the influence of grain boundary on cerium substituted Nd–Fe–B magnets *AIP Adv.* **7** 056201
[32] Hono K and Sepehri-Amin H 2012 Strategy for high-coercivity Nd–Fe–B magnets *Scr. Mater.* **67** 530–5